Dalton Transactions

ROYAL SOCIETY OF CHEMISTRY

PAPER

View Article Online
View Journal

Cite this: DOI: 10.1039/d1dt02359d

Comparing coordination uranyl(VI) complexes with 2-(1*H*-imidazo[4,5-*b*]phenazin-2-yl)phenol and derivatives†

E. A. Hiti,[a] G. R. Wilkinson,[a] I. R. Ariyarathna,[a,b] C. D. Tutson,[a] E. E. Hardy,‡[a] B. A. Maynard,[a] E. Miliordos*[a] and A. E. V. Gorden*[a,c]

Received 15th July 2021,
Accepted 21st July 2021

DOI: 10.1039/d1dt02359d

rsc.li/dalton

Four derivatives of 2-(1*H*-imidazo[4,5-*b*]phenazin-2-yl)phenol have been synthesized and characterized structurally using X-ray crystallography. Coordination complexes with uranyl (UO_2^{2+}) and copper (Cu^{2+}) were prepared and absorption/emission spectra detailed. We observed increased fluorescence upon uranyl binding, in stark contrast to rapid quenching observed with the addition of copper. These phenomena have been further examined by DFT computational methods.

Introduction

Imidazole and benzimidazole-containing ligands are naturally present in biomolecules and have been found to be pertinent to biological and medical applications demonstrating anti-inflammatory and anti-tumour activities.[1,2] Complexes with two such ligands display π–π interactions,[3] while benzimidazole derivatives have been used in polymer enhancing catalysis and as fluorescent probes to detect Fe(III) and nitric oxide.[4–7] Imidazole-containing d- and f-block metal complexes have been reported for use in organic light-emitting diodes (OLEDs).[8,9] Specific benzimidazole derivatives act as bidentate ligands exhibiting an N–C–C–C–O binding motif (N and O atoms connected with a three-C bridge coordinate to the metal). Complexes with these ligands have been reported with first row transition metals such as copper, nickel, and iron.[10,11] Other research has demonstrated that ligands can take advantage of soft donors like imine nitrogens such as these in coordination of the actinides.[12–16]

The ligand 2-(1*H*-imidazo[4,5-*b*]phenazin-2-yl)phenol (dubbed "salimidizine") represents a class of benzimidazole derivatives with extended conjugation and presents a potential means to investigate coordination by comparing emission properties. This ligand was first reported by Amer and co-workers in 1999,[17] and it was later spectroscopically characterized in 2011 by Lei and co-workers with various substituents on the terminal benzene ring (X = H, CH_3O, CH_2OH, Br, and Cl).[18] Here, we report crystal structures and spectroscopic characterization for this ligand and its coordination complexes with uranyl (UO_2^{2+}) and copper (Cu^{2+}). These ligand frameworks have been shown to be good fluorescence sensors for both organic molecules and metal ions, in most cases as a "turn off" sensor.[7,19,20] In this study, we demonstrate the ability of uranyl coordination to enhance the emission intensity of the system to help distinguish between metal ions. Uranyl and copper were selected for comparison in this study because of their +2 oxidation states, their similar charge to ionic radius ratios, and their competitive binding behavior in an attempt to characterize clear distinctions between the two metal ions. We observed that upon coordination of uranyl, fluorescence intensity increases, but decreases dramatically for copper coordination showing a marked difference which is notable in other systems proposed or characterized with an interest in uranyl detection.[21–24]

Salimidizine, and three derivatives thereof, were prepared through a condensation reaction between a salicylaldehyde and 2,3-diaminophenazine followed by a subsequent intramolecular cyclization reaction, affording **L1** (salimidizine), **L2** (*t*-butylsalimidizine), **L3** (cyanosalimidizine), and **L4** (methoxysalimidizine) in moderate yields (Scheme 1). To understand better the different ligand–metal interactions with UO_2^{2+} and Cu^{2+}, quantum chemical calculations were performed to describe the ground and excited electronic states of their complexes with **L1**.

[a]*Department of Chemistry and Biochemistry, Auburn University, Auburn, AL 36849, USA*
[b]*Department of Chemical Engineering, Massachusetts Institute of Technology, Cambridge, MA 02139, USA*
[c]*Department of Chemistry and Biochemistry, Texas Tech University, Lubbock, TX 79409, USA. E-mail: anne.gorden@ttu.edu*

†Electronic supplementary information (ESI) available: Crystallographic details, spectroscopic, and spectrometric characterization data. CCDC 1946969, 2015766 and 2067348. For ESI and crystallographic data in CIF or other electronic format see DOI: 10.1039/d1dt02359d

‡Current address: Department of Chemistry, Old Dominion University, Norfolk, VA 23529, USA.

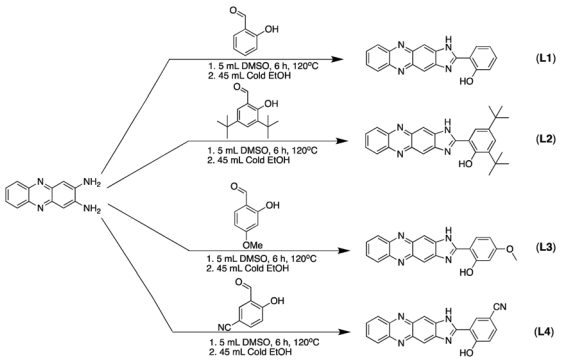

Scheme 1 Synthetic scheme for ligands **L1**, **L2**, **L3**, **L4**.

Results and discussion

Crystallographic data

Projections of the free-base ligands **L1** and **L2**, as crystalized from slow evaporation of THF, are shown in Fig. 1 and 2, respectively. The O1–N1 distance in[**L1**]UO_2(OAc)(DMSO) is 2.767(9) Å, which is larger in comparison to the O1–N1 distance of 2.587(19) Å in **L1**. Upon binding of this bidentate O–N binding site, the O–N distance expands to accommodate the metal. The O1–N1 distance in **L2** is 2.557 (18) Å, which is comparable to **L1**. Complete crystallographic data tables and all bond lengths and angles are available in ESI.†

Metal complexes with these ligands were obtained through layering of a metal salt solution with a solution of the free base ligand **L1**. Fig. 3 shows a projection of [**L1**]UO_2(OAc)(DMSO), which was crystallized through slow diffusion of hexanes into a layered solution of free base ligand **L1** dissolved in DMSO and $UO_2(OAc)_2$ in EtOH. The uranium center in [**L1**]UO_2(OAc)(DMSO) is seven coordinate and shown to have a pentagonal bipyramidal geometry. Six oxygen atoms in total and one nitrogen atom occupy these seven coordination sites. The first two coordinating oxygen atoms are the terminal oxo groups of the UO_2^{2+} subunit; the three additional oxygen atoms can be accounted for by the coordination of a DMSO solvent molecule and an acetate anion. The remaining oxygen and nitrogen atoms that fill the coordination sphere of the uranium are from the salimidizine ligand. The U–N distance is observed at 2.558(6) Å. The U–O distance is observed at 2.220 (6) Å. These distances are quite comparable to other Schiff base complexes that are found to contain 5 coordinate uranyl metal centers (Table 1).[16,25,26]

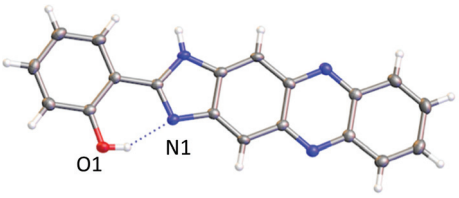

Fig. 1 Projection of the asymmetric unit of **L1**. Atoms as shown are labelled: H in white, O in red, N in blue, and C in grey.

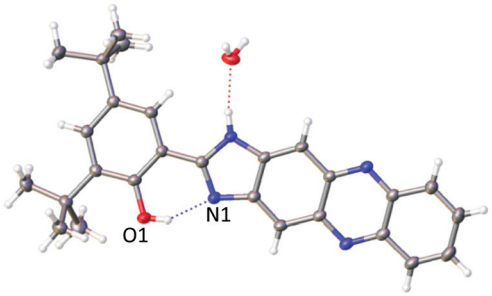

Fig. 2 Projection of the asymmetric unit of **L2**. Atoms as shown are labelled: H in white, O in red, N in blue, and C in grey.

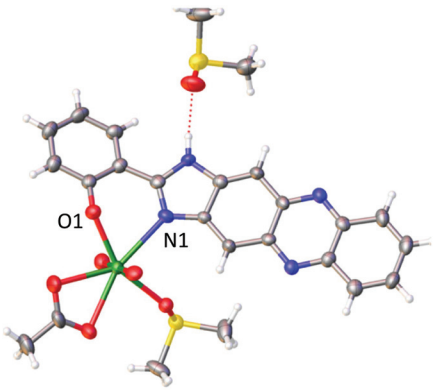

Fig. 3 Projection of the asymmetric unit of [**L1**]UO_2(OAc)(DMSO). Atoms shown are labelled: H in white, O in red, N in blue, C in grey, S in yellow, U in green.

UV-vis spectral data

Because of low solubility, solution studies were performed using a batch titration method for all four ligands. Stock solutions of **L1**, **L2**, **L3**, and **L4** were made to 0.001 M solution of ligand in 40 mL of dimethylformamide (DMF). Metal stock solutions of both Cu^{2+} and UO_2^{2+} as the acetate salts were made to be 0.001 M in 25 mL of DI H_2O. Each batch of ligand measurements contained a ligand blank solution with no metal followed by 14 additional samples containing 1 equivalent of ligand, subsequently introducing 0.1 equivalents of metal stock solution up to 1 equivalent of metal. After reaching 1 equivalent of metal, additional equivalents were added until achieving 5 equivalents of metal. All samples were prepared, and 1 μL of 0.1 M trimethylamine (TEA) in DMF was added to each of the samples to facilitate deprotonation. All samples were diluted to 5 mL in volume such that they contained 10% H_2O in DMF. The samples were prepared, and then allowed to sit for 24 hours before spectra were collected.

Table 1 Crystallographic data fr **L1**, **L2** & UO_2[**L1**](OAc)·DMSO

Parameters	**L1**	**L2**	[**L1**]UO_2(OAc)(DMSO)
Formula	$C_{19}H_{12}N_4O$	$C_{31}H_{38}N_4O_3$	$C_{25}H_{26}N_4O_7S_2U$
Formula weight	312.33	514.65	796.65
Crystal system	Monoclinic	Triclinic	Monoclinic
Space group	$P2_1/n$	$P\bar{1}$	$P2_1/n$
a [Å]	6.6597(6)	9.0812(5)	8.585(5)
b [Å]	30.064(3)	9.9887(5)	20.419(11)
c [Å]	7.2617(6)	16.3825(9)	16.091(9)
α [°]	90°	103.5190(10)°	90°
β [°]	108.293(2)°	103.2200(10)°	101.633(8)°
γ [°]	90°	99.4900(10)°	90°
V [Å^3]	1380.4(2)	1368.65(13)	2763(3)
h, k, l (max)	8, 39, 9	12, 13, 21	10, 25, 20
Z	4	2	4
ρ_{calc} g cm^{-3}	1.5027	1.249	1.915
F(000)	648.3	552	1536
θ Min–Max [°]	5.42–54.96	2.15–28.70	3.26–53.14
Independent reflections	3173	7073	4613
$R_{(int)}$	0.0386	0.0336	0.0639
Final R indexes [$I > 2\sigma(I)$]	R_1 = 0.0582, wR_2 = 0.1239	R_1 = 0.0489, wR_2 = 0.1266	R_1 = 0.0450, wR_2 = 0.1157
Final R indexes [all data]	R_1 = 0.0784, wR_2 = 0.1332	R_1 = 0.0686, wR_2 = 0.1411	R_1 = 0.0602, wR_2 = 0.1281
GOF on F^2	1.067	1.054	1.069

Additional titration experiments with the bare ligand, salimidizine (**L1**), were performed with UO_2^{2+} and with Cu^{2+}. Some of the individual spectra were removed for clarity but full spectra can be seen in the Fig. S9–S18 in the ESI.† The UV-vis spectra showed a peak at 439 nm characteristic of the bare ligand, and no additional shifts were detected after subsequent additions of UO_2^{2+}, even after the addition of 5 full equivalents of metal and 24 hours of reaction time. The only observed spectral change involved a small increase in absorbance with each equivalent of metal added (Fig. S12†). The Cu^{2+} titration showed a much more dramatic shift in the spectra as λ_{max} shifted bathochromically from 416 nm to 455 nm after addition of the first 0.1 equivalent and remains unchanged until a ratio of 1 : 1 ligand to metal was reached. Between addition of the second equivalent of metal and up to 5 equivalents λ_{max} shifts hypsochromically to 325 nm (Fig. 5). Although there was no significant shift in the spectra that would suggest binding of the uranyl by **L1** under these conditions, we were able to obtain a crystal structure of the **L1** ligand bound to the uranyl.

Upon further examination, the UV-Vis data of solutions containing the ditertbutyl-salimidizine ligand were most promising in terms of metal coordination. The addition of base was required to facilitate coordination, as was made evident from the observed spectral shifts. Ditertbutylsalimidizne (**L2**) coordination with UO_2^{2+} was observed by batch titration, and the following features were observed: the ligand free base showed a peak centred at 421 nm and after the first 0.1 equivalents of metal were added, a shift to 440 nm was noticed. This change intensified, but was not fully defined, until 0.3 equivalents were added to the sample (Fig. 4). This bathochromic shift seemed to demonstrate that a binding event had occurred; however, the solutions showed no visible colourimetric change as all samples exhibited a similar pale yellow colour (Fig. S12†).

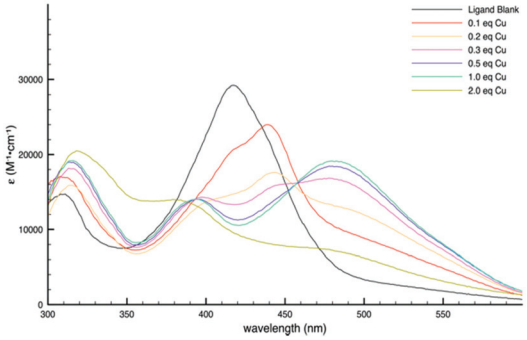

Fig. 4 Ditertbutylsalimidizine (**L2**) titration with Cu(II) acetate and triethylamine.

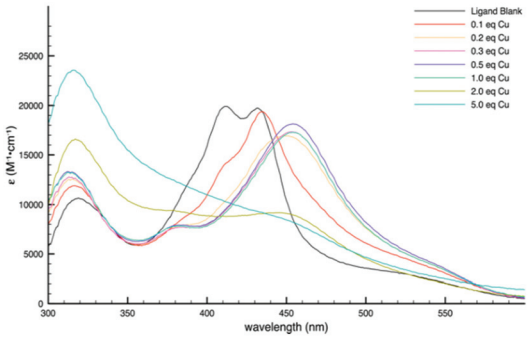

Fig. 5 Salimidizine (**L1**) titration with Cu^{2+} and triethylamine.

This ligand (**L2**) also demonstrated some affinity for Cu^{2+}. The titrations of **L2** with copper showed significant changes with increases in metal ion concentration. Upon addition of 0.1 to 0.7 equivalents of Cu^{2+} the resulting solutions retained a yellow colour. With the additions of 0.8 to 1.0 equivalents of metal, there was a 64 nm bathochromic shift in the spectral trace, and the solutions turned a rose gold colour. From 2.0 to 5.0 equivalents of metal the solutions went back to a yellow colour, although this was different than the earlier colouration. Further examination of the UV-vis spectra (Fig. 6) demonstrated that the initial signal of the ligand centred at 421 nm demonstrated a bathochromic shift when the first 0.1 equivalents of metal was added. Upon addition of 0.4 equivalents, the initial signal was completely shifted with a maximum absorptivity now located at 485 nm. Looking at the absorbance *vs.* equivalents graph (Fig. S8†) it is evident that the shift starts after base and the first 0.1 equivalent of metal solution were added. The addition of base was needed to help with deprotonation of the ligand. The subsequent spectral shifts either were not observed or occur at a very slow rate without further addition of base.

Further examination of methoxysalimidizine (**L3**) titrated with Cu^{2+} showed a λ_{max} for the ligand centred at 425 nm

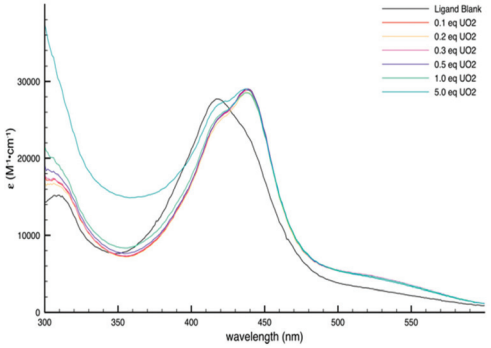

Fig. 6 Ditertbutylsalimidizine (**L2**) titration with UO_2^{2+} acetate and triethylamine.

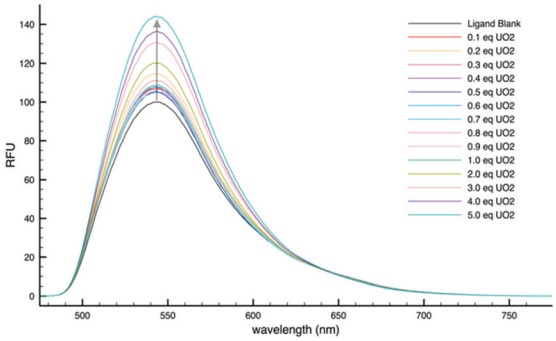

Fig. 8 Fluorescence spectra of salimidizine (**L1**) with UO_2^{2+} acetate in DMF/10% H_2O.

(Fig. S15†). After the addition of the first equivalent of metal, it was found to shift bathochromically to its new location at 463 nm. Along with this shift, after 2 full equivalents of metal are added the molar absorptivity in the λ_{max} starts to decrease in intensity. When titrated with UO_2^{2+}, the peak initially had a λ_{max} centred at 425 nm and after the first addition of metal, the peak shifts to 441 nm where it was found to remain, regardless of the subsequent additions.

Fluorescence data

These ligand frame works have been shown to have excellent fluorescence characteristics due to their highly conjugated structure. There are a few important details observed in the fluorescence spectra that should be noted. These titrations were carried out in DMF with 10% H_2O for $Cu^{2+}(OAc)_2$ and UO_2^{2+} (OAc) similar to the batch UV-vis titrations. The bare salimidizine ligand showed some interesting features upon the introduction of metal. For the ligand alone, with excitation at 408 nm, a major peak was produced at 536 nm. After the first addition of Cu^{2+} solution (0.1 equivalents), the emission intensity starts to decrease from 100 Raw Fluorescence Units (RFU) and this continues with each addition of the metal solution to the lowest point at 15 RFU after the addition of 5 equivalents of metal (Fig. 7).

More interesting observations that can be made from the fluorescence spectra come from the UO_2^{2+} titrations with the salimidizine ligand. In this case, the initial peak is centred at 540 nm with an intensity of 100 RFU. Upon addition each aliquot of metal solution, the signal intensified to reach 140 RFU (Fig. 8). It can also be noted that this trend holds across all the functionalized salimidizines and can be further examined in the ESI Fig. S19–S26.† Overall, the distinctive change in fluorescence intensity is quite remarkable in comparing the copper and uranyl complexes.

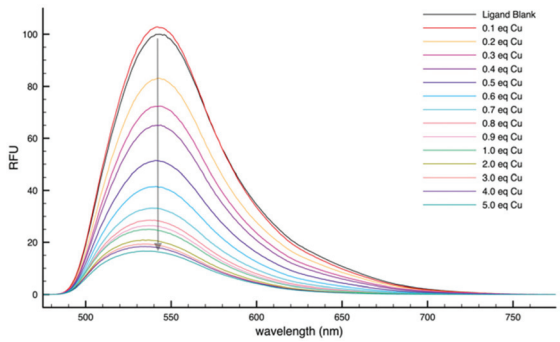

Fig. 7 Fluorescence spectra of salimidizine (**L1**) with Cu^{2+} acetate in DMF/10% H_2O.

Calculations

To explain the opposite activity of the uranyl and copper(II) metal ions upon complexation, we first optimized the structure of the two complexes with **L1** at their singlet (uranyl) and doublet (copper) ground states. To complete the first coordination sphere of the metals, we added an acetate (AcO) and/or a water (W) ligand, constructing totally four complexes: $L_1UO_2^{2+}$ (AcO), $L_1UO_2^{2+}$ (AcO)(W), L_1Cu^{2+} (AcO), and L_1Cu^{2+} (AcO)(W). The copper and uranyl structures used for the calculations were derived from the crystal structure of [**L1**]UO_2(OAc)(DMSO). Both metals were coordinated by the ligand and an (AcO) counter ion to achieve a neutral species. The water is placed to better reflect the conditions of the spectroscopy experiments and is also needed in the case of the uranyl to fill its fifth coordination site. This enabled us to see the possible effect of the coordination of different solvent molecules. All of our optimized geometries are given in the ESI (Table S1†). Using this geometry, we employed TD-DFT to identify the state with the highest oscillator strength in the region of the absorption frequency used for the experiments (416 nm). The tenth state showed the only non-zero oscillator strength in this region for all cases except $L_1UO_2^{2+}$ (AcO)(W), for which it was the eleventh state (always of the same spin as the ground state). The theoretical absorption wavelengths were 415 and 419 nm for the two uranyl complexes, and 455, 466 nm for the copper ones. These numbers show the little effect of the solvent coordination.

Next, we optimized the geometry of this excited state, and we calculated the emission wavelength as the excitation energy of this state at its optimal geometry. It should be mentioned that, after optimization, the highest oscillator strength state is

the fifth and sixth excited state for the uranyl and copper complexes, respectively. In every case, the excitation corresponds to a ligand–ligand electron transfer. The contours of the natural transition orbitals for the $L_1UO_2^{2+}$ (AcO)(W) and L_1Cu^{2+} (AcO) molecules shown in Fig. 8 are representative for the uranyl and copper systems, respectively. For copper, the electron transition is clearly a ligand-to-ligand transition. For uranyl, the same ligand to ligand transition has substantial involvement of some f-orbital or uranium.

The geometries of the two states differ mainly in the distances of the metal and connected oxygen or nitrogen atoms belonging to L1. Going from the ground to the excited state geometry, U–O distances increase by about 0.2 Å but U–N shorten by 0.04 Å. Likewise, Cu–O distances increase by 0.08 Å for both L_1Cu^{2+} (AcO) and L_1Cu^{2+} (AcO)(W) complexes, but the Cu–N distances are not affected at least within 0.01 Å.

The calculated emission wavelengths of 562 (L_1Cu^{2+} (AcO)), 600 (L_1Cu^{2+} (AcO)(W)), 599 (L_1Cu^{2+} (AcO)), and 607 ($L_1UO_2^{2+}$ (AcO)(W)) nm are overestimated relative to the experimental peak maxima, but are in reasonable agreement given the absence of solvent effects and the accuracy of TD-DFT. We then, constructed the potential energy profile of the first ten or eleven electronic states of each complex along the "reaction" coordinate connecting the minima of the ground and high oscillator strength excited electronic state (see Fig. 9). As in Fig. 8, the $L_1UO_2^{2+}$ (AcO)(W) and L_1Cu^{2+} (AcO) molecules have been selected for Fig. 9. Comparison of the two potential energy profiles makes clear the reason for the observed fluorescence quenching in the copper case. For uranyl, the initial excitation (left orange arrow) to the non-zero oscillator strength excited state is followed by relaxation to its minimum *via* a series of conical intersections (upper grey arrow). Radiative decay to ground state (right yellow arrow) generates the recorded fluorescence signal and the system returns to the global minimum of the ground state in a non-radiative manner (lower grey arrow). The same process can, in principle, occur for copper, but the minimum of the pertinent excited state is shallow. The molecule after a small energy barrier goes to a lower minimum of the same potential energy surface, which has nearly zero oscillator strength, and the decay to the ground state happens in a non-radiative manner. Notice that uranyl has also a second minimum in the excited state, which however is higher in energy. The profiles for all four systems (uranyl/copper acetate and/or water) are shown in the ESI.† Coordination of water destabilizes the excited state geometry in both cases and enhances the fluorescence quenching in the copper case (Fig. 10).

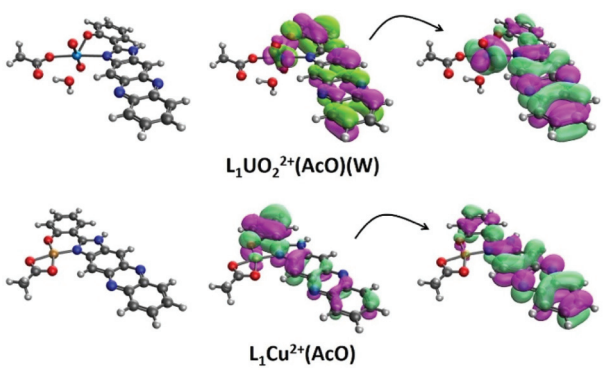

Fig. 9 Natural transition orbitals corresponding to the excitation from the ground state to the lowest excited state of $L_1UO_2^{2+}$ (AcO)(W) and L_1Cu^{2+} (AcO) with non-zero oscillator strength.

Materials and methods

Organic solvents were used as received without additional purification. 2,3-Diaminophenazine was obtained from Sigma-Aldrich, salicylaldehyde and 2-hydroxy-4-methoxybenzaldehyde were obtained from Acros Organics, 3,5-di-*tert*-butylsalicylaldehyde was obtained from TCI and used without further purification. 2-Hydroxy-5-cyanobenzaldehyde was prepared following a procedure from Suzuki and Takahashi.[27] Copper(II) acetate salt was obtained from Strem Chemicals, and uranyl(II) acetate

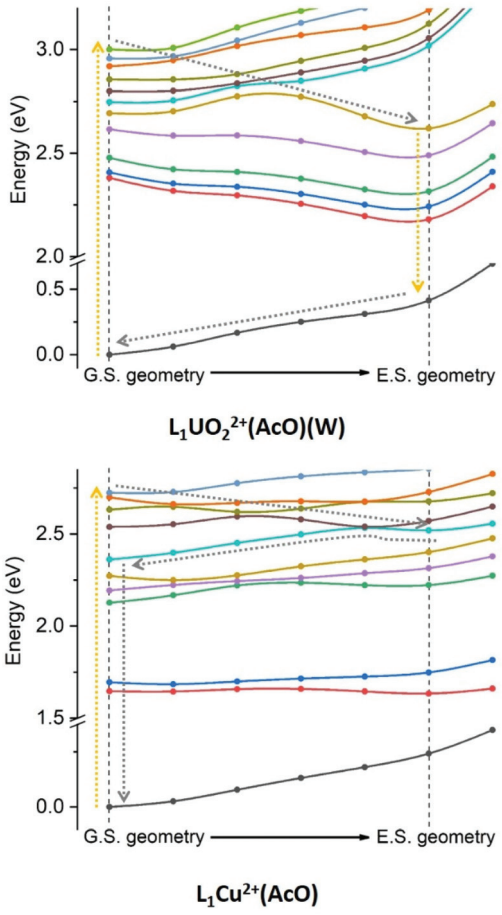

Fig. 10 Potential energy profiles of the lowest lying electronic states of $L_1UO_2^{2+}$ (AcO)(W) and L_1Cu^{2+} (AcO) along the path connecting the geometries of ground state (G.S. geometry) and the excited state (E.S. geometry) with non-zero oscillator strength. Orange and grey arrows indicate radiative and non-radiative transitions.

salt was obtained from Polysciences, and these were used without further purification.

Caution! The $UO_2(C_2H_3O_2)_2{\cdot}2H_2O$ used in this study contained depleted uranium, standard precautions for handling radioactive materials or heavy metals, such as uranyl nitrate, and uranyl acetate were followed.

Apparatus

^1H and ^{13}C NMR were recorded on a Bruker AV 400 or 600 MHz spectrometer using $(CD_3)_2SO$ and DMF-d_7 (Cambridge Isotope Laboratories) as indicated. Chemical shifts are reported in parts per million (δ) and are referenced against residual internal solvent signals or with respect to tetramethyl silane (TMS) as the internal standard. Purities of compounds have been established *via* NMR and elemental analysis. The UV-Vis data was collected on a Varian Cary 50 WinUV spectrophotometer. Infrared spectra were obtained in the solid state using an attenuated total reflectance (ATR) method on a Thermo Scientific Nicolet iS50 FT-IR instrument. Suitable crystals were selected and mounted on a glass fiber using paratone-n oil and data collection was completed on a 'Bruker APEX CCD' diffractometer using Mo Kα radiation. The crystals were kept at 180(2) K during unit cell and data collection. SMART (v. 5.624) was used for preliminary determination of cell constants and data collection control. Determination of integrated intensities and global cell refinements were performed with the Bruker SAINT software package, and empirical absorption corrections (SADABS) were applied. The structure was solved with the ShelXS structure solution program using Direct Methods[28] and refined with the olex2.refine[29] refinement package using Gauss–Newton minimization. Projections were created on Olex2 software.[29]

Density Functional Theory (DFT) calculations were performed to obtain the optimal geometry of the **L1** complexes with UO_2^{2+} and Cu(II). The B3LYP functional[30,31] combined with the cc-pVDZ basis sets[32,33] for C, N, O, H, Cu, and cc-pVDZ-PP basis set[34] for U (60 inner electrons are replaced by the Stuttgart relativistic pseudopotential). Excited electronic states were examined with the time dependent DFT (TD-DFT) approximation. All calculations were done with Gaussian 16.[35]

Synthesis and characterization

Ligand synthesis

Synthesis of 2-(1*H*-imidazo[4,5-*b*]phenazin-2-yl)phenol (salimidizine, L1). 2,3-Diaminophenazine (0.6 mmol; 0.1261 g) was stirred into 5 ml of DMSO in a 50 mL round bottom flask to dissolve. Next, salicylaldehyde (0.0006 mol;53 μL) was added to the stirring mixture. The reaction was heated to 120 °C, and allowed to react for 6 h. The reaction was then removed from heat and allowed to cool to room temperature. Next, 45 ml of chilled EtOH was added to the reaction mixture to help the product precipitate out of solution. The solution was allowed to sit at 0 °C overnight in the freezer, then filtered and washed with cold EtOH. The resulting solid was filtered from the solution, then placed in the vacuum oven overnight to remove any excess solvent. Yield: 85%. NMR (600 MHz, DMF-d7, ppm): 13.84 (s, 1H), 13.17 (s, 1H), 8.32–8.48 (m, 4H), 8.24 (m, 2H), 7.91 (s, 2H), 7.57 (m, 1H), 7.13–7.17 (m, 2H). FT-IR (ATR): 2900 cm^{-1} (νR–CH), 3100 cm^{-1} (νR–OH), 3300 cm^{-1} (νR–NH) ESI + MS *m*/*z* (M + H): calc: 313.1079; found: 313.1076.

Synthesis of 2,4-di-*tert*-butyl-6-(1*H*-imidazo[4,5-*b*]phenazin-2-yl)phenol (DTB sutylsalimidizine, L2). 2,3-Diaminophenazine (0.6 mmol; 0.1261 g) was stirred into 5 ml of DMSO and allowed to dissolve. Next, 3,5-ditertbutylsalicylaldehyde (0.5 mmol; 0.1172 g) was added to the stirring mixture. The reaction was heated to 120 °C, and allowed to react for 6 h. The reaction was then removed from heat and allowed to cool to room temperature. Next, 45 ml of chilled EtOH was added to the reaction to help the product precipitate out of solution. The solution was allowed to sit at 0 °C overnight in the freezer, then filtered and washed with cold EtOH. The filtered solid was then placed in the vacuum oven for 16 hours to remove any excess solvent (0.0971 g). Yield: 38%. NMR (600 MHz, DMF-d7, ppm): δ 14.10(1H, s), 8.25–8.60 (5H, m), 7.94–7.95 (2H, m), 7.63 (1H, s), 1.55 (9H, s), 1.42 (9H, s). FT-IR (ATR): 1400 cm^{-1} (νR–CH), 1650 cm^{-1} (νR–C═C), 3150 cm^{-1} (νR–OH). ESI + MS *m*/*z* (M + H): calc: 425.2346; found: 425.2341.

Synthesis of 2-(1*H*-imidazo[4,5-*b*]phenazin-2-yl)-5-methoxyphenol (methoxysalimidizine, L3). 2,3-Diaminophenazine (0.6 mmol; 0.1261 g) was stirred in 5 ml of DMSO in a 50 mL round bottom flask to dissolve. Next, 2-hydroxy-4-methoxybenzaldehyde (0.5 mmol;0.0761 g) was added to the stirring mixture. The reaction was heated to 120 °C and allowed to react for 6 h. The reaction was then taken off heat and allowed to cool to room temperature, then 45 ml of chilled EtOH was added to the reaction to help the product precipitate out of solution. The solution was allowed to sit at 0 °C in a freezer overnight, then filtered and washed with cold EtOH. The filtered solid was then placed in the vacuum oven overnight to remove any excess solvent (0.0847 g). Yield: 49%. NMR (600 MHz, DMF-d7, ppm): δ 13.47 (s, 1H), 8.33 (s, 2H), 8.21 (s, 3H), 8.02 (s, 1H), 7.88 (s, 2H), 6.72–6.68 (m, 2H), 3.92 (m, 3H). FT-IR (ATR): 1100 cm^{-1} (νR–C–O), 1650 cm^{-1} (νR–C═C), 2900 cm^{-1} (νR–CH), 3100 cm^{-1} (νR–OH), 3300 cm^{-1} (νR–NH). ESI − MS *m*/*z*(M − H): calc: 341.1044; found: 341.1182.

Synthesis of 4-hydroxy-3-(1*H*-imidazo[4,5-*b*]phenazin-2-yl) benzonitrile (for cyanosalimidizine, L4). 2,3-Diaminophenazine (0.6 mmol; 0.1261 g) was stirred in 5 ml of DMSO in a 50 mL round bottom flask to dissolve. Next, 2-hydroxy-5-cyanobenzaldehyde (0.5 mmol; 0.0736 g) was added to the stirring mixture. The reaction was heated to 120 °C and allowed to react for 6 h. The reaction was then removed from heat and allowed to cool to room temperature. Then, 45 ml of chilled EtOH was added to the reaction to help the product precipitate from solution. The solution was allowed to sit at 0 °C in a freezer overnight, then filtered and washed with cold EtOH. The filtered solid was then placed in the vacuum oven overnight hours to remove any excess solvent

(0.1467 g). Yield: 86%. NMR (400 MHz, DMSO, ppm): δ 13.65 (s, 2H), 8.64 (s, 1H), 8.41 (s, 2H), 8.19 (d, 2H), 7.71–8.10 (m, 3H), 7.12 (d, 1H). FT-IR (ATR): 1650 cm^{-1} (νR–C═C), 2200 cm^{-1} (νC≡N), 3050 cm^{-1} (νR–OH), 3300 cm^{-1}(νR–NH). ESI + MS m/z(M + H): calc: 338.1030; found: 338.1028.

Synthesis of 2-hydroxy-5-cyanobenzaldehyde. 4-Hydroxybenzonitrile (0.020 mol; 2.38 g) was dissolved in 8 mL of trifluoroacetic acid. Once dissolved, hexamethylenetetraamine (0.040 mol; 5.61 g) was added to the solution. Gas will evolve upon addition and should be allowed to dissipate. The mixture was heated to 100 °C, and allow to react for 7 h. The reaction mixture was removed from heat and put directly in an ice bath for 5 min. The reaction mixture was removed from the ice bath and allow to warm to room temperature. Once at room temperature, 10 mL of 50/50 solution of H_2SO_4/H_2O was added to the reaction mixture followed by 60 mL of H_2O. The solution was allowed to stir at room temperature for 30 min. After the 30 min, a light-yellow solid formed in the solution. The solid was filtered off and the mother liquor was extracted with CH_2Cl_2. The organic layer was separated and placed in the refrigerator to allow for recrystallization to allow for recrystallization (0.9080 g). Yield: 31%. NMR (400 MHz, DMSO, ppm): δ 13.55 (s, 1H), 8.58 (s, 1H), 8.35 (m, 2H), 8.13 (m, 3H), 7.82 (m, 3H), 7.21 (m, 1H). FT-IR (ATR): 1670 cm^{-1} (νC═O), 2230 cm^{-1} (νC≡N), 3207 cm^{-1} (νR–OH).

Synthesis of salimidizine (L1)-Cu complex. (**L1**) (0.049 mmol; 15.3 mg) was dissolved in 50 mL of THF and was allowed to stir for 20 min at 50 °C to help dissolve the ligand. Next, 20 mL of MeOH was added to the reaction mixture followed by anhydrous $Cu(OAc)_2$ (0.049 mmol; 9.0 mg), and triethylamine (0.098 mmol; 20 μL) to assist with deprotonation. The reaction was heated to 60 °C for 48 hours. The reaction was followed by TLC by 3 : 1 EtOAc : hexane mixture. The reaction mixture was taken off heat and was then taken to dryness under reduced pressure yielding a brown/black solid the solid was scraped from the round bottomed flask and washed with EtOH and filtered (21.3 mg). Yield: 96%. FT-IR (ATR): 1650 cm^{-1} (νR–C═C), 2900 cm^{-1} (νR–CH), 3300 cm^{-1} (νR–OH_2), 3650 cm^{-1}(νR–NH) ESI + MS m/z(M + K): calc: 591.1309, found; 591.0868; elemental analysis: calc: C (54.17), H (3.56), N (11.35); found C (54.43), H (3.69), N (11.35). Formula: $C_{23}H_{16}N_4O_5Cu\cdot(H_2O)$.

Synthesis of salimidizine (L1)-UO_2 complex. (**L1**) (0.049 mmol; 15.3 g) was dissolved in a mixture of 30 mL THF/15 mL MeOH and was allowed to stir for 20 min at 40 °C to help dissolve the ligand. Next, uranyl acetate dihydrate (0.049 mol; 21.0 mg) was added to the reaction, followed by triethylamine (0.000098 mol; 20 μL) to assist in deprotonation of the ligand. The reaction was heated to 60C and allowed to react for 48 hours. The reaction was then taken to dryness under reduced pressure by means of a rotary evaporator to yield a brown/red solid. The solid was scraped from the round bottomed flask and washed with EtOH and filtered (11.1 mg). Yield: 34%, NMR (500 MHz, DMF-d7, ppm): δ8.49 (s, 1H), 8.39–8.28 (m, 5H), 7.92 (s, 1H), 7.66–7.47 (m, 3H), 7.16 (d, 3H), 6.97–6.65 (m, 2H), 1.40 (s, 3H). FT-IR (ATR): 850 cm^{-1} (νR–O═U═O), 1600 cm^{-1} (νR–C═C), 2900 cm^{-1} (νR–CH), 3450 cm^{-1} (νR–NH), 3500 cm^{-1} (νR–OH_2). ESI + MS m/z(M + K): calc: 737.1402, found: 737.5061. Elemental analysis: calc: C (36.90), H (2.70), N (6.89); found C (36.64), H (2.72), N (6.53). Formula: $C_{21}H_{15}N_4O_6U\cdot2(C_2H_6OS)$.

Synthesis of DTB salimidizine (L2)-Cu complex. (**L2**) (0.049 mmol; 20.7 mg) was dissolved in a mixture of 30 mL DMF/15 mL MeOH and was allowed to stir for 20 min at 40 °C to help dissolve the ligand. Next, copper(II) acetate (0.049 mmol; 9.0 mg) was added to the reaction, followed by triethylamine (0.098 mmol; 20 μL) to assist in deprotonation of the ligand. The reaction was heated to 66 °C and allowed to react for 48 hours. The reaction was followed by TLC by 3 : 1 EtOAc : hexane mixture. The reaction was then taken to dryness under reduced pressure by rotary evaporation to yield a brown/red solid the solid was scraped from the round bottom and washed with EtOH and filtered (26.2 mg). Yield: 97%. FT-IR (ATR): 1650 cm^{-1} (νR–C═C), 2900 cm^{-1} (νR–CH), 3100 cm^{-1} (νR–NH), 3400 cm^{-1} (νR–OH_2) ESI + MS m/z(M + H): calc: 547.138, found: 548.1805. Elemental analysis: calc: C (60.81), H (5.98), N (10.13); found C (60.68), H (5.59), N (10.53). Formula: $C_{31}H_{32}N_4O_5Cu\cdot(C_4H_9NO)$.

Synthesis of DTB salimidizine (L2)-UO_2 complex. (**L2**) (0.049 mmol; 15.3 mg) was dissolved in a mixture of THF/MeOH and was allowed to stir for 20 min at 40 °C to help dissolve the ligand. Next uranyl acetate dihydrate (0.049 mmol; 21.0 mg) was added to the reaction, followed by triethylamine (0.098 mmol; 20 μL) to assist in deprotonation of the ligand. The reaction was heated to 660C and allowed to react for 48 hours. The reaction was followed by TLC by 3 : 1 EtOAc : hexane mixture. The reaction was then taken to dryness under reduced pressure to yield a brown/red solid the solid was scraped from the round bottom and washed with EtOH and filtered (23.5 mg). Yield: 62%, NMR (500 MHz, DMF-d7, ppm): δ 8.59 (s, 1H), 8.32–8.26 (m. 3H), 7.94–7.92 (dd, 3H, J = 3.3, 3.5), 7.62 (d, 1H, J = 2.2), 1.80 (s, 3H), 1.54 (s, 9H), 1.41 (s, 9H). FT-IR (ATR): 900 cm^{-1} (νR–O═U═O), 1650 cm^{-1} (νR–C═C), 2900 cm^{-1} (νR–CH), 3200 cm^{-1} (νR–OH_2). ESI + MS m/z(M + Na): calc: 911.305, found; 911.3776. Elemental analysis: calc C (45.93), H (3.98), N (6.91); found C (46.28), H (4.19), N (6.69). Formula: $C_{31}H_{34}N_4O_7U$.

Synthesis of OMe salimidizine (L3)-Cu complex. (0.049 mmol; 17.5 mg) was dissolved in a mixture of 12 mL DMF/8 mL of H_2O and was allowed to stir for 20 min at 50 °C to help dissolve the ligand. Next copper(II) acetate (0.049 mmol; 9.0 mg) was added to the reaction, followed by triethylamine (0.098 mmol; 20 μL) to assist in deprotonation of the ligand. The reaction was heated to 1000C and allowed to react for 48 hours. The reaction was followed by TLC by 3 : 1 EtOAc : hexane mixture. The reaction was then taken to dryness under high vac at 70 °C to yield a black solid the solid was scraped from the round bottom and washed with EtOH and filtered (11.9 mg). Yield: 52%. FT-IR (ATR): 1650 cm^{-1} (νR–C═C), 2900 cm^{-1} (νR–CH), 3300 cm^{-1} (νR–OH_2), ESI + MS m/z(M + H): calc: 539.063, found: 539.0908; elemental analysis:

calc: C (54.94), H (3.56), N (11.65); found C (55.20), H (3.61), N (12.02). Formula: $C_{22}H_{15}N_4O_4Cu\cdot(H_2O)$.

Synthesis of OMe salimidizine (L3)-UO_2 complex. (**L3**) (0.050 mmol; 17.2 mg) was dissolved in a mixture of 12 mL DMF/8 mL of H_2O and was allowed to stir for 20 min at 50 °C to help dissolve the ligand. Next uranyl acetate dihydrate (0.05 mmol; 21.0 mg) was added to the reaction, followed by triethylamine (0.098 mmol; 20 μL) to assist in deprotonation of the ligand. The reaction was heated to 100 °C and allowed to react for 48 hours. The reaction was followed by TLC by 3 : 1 EtOAc : hexane mixture. The reaction was then taken to dryness under high vaccuum at 70 °C to yield a brown solid. The solid was scraped from the round bottomed flask and washed with EtOH and filtered (28.3 mg). Yield: 83%, NMR (500 MHz, DMSO, ppm): δ8.95 (s, 1H), 8.30–8.12 (m, 3H), 7.86 (s, 3H), 6.63 (s, 1H), 6.45 (s, 1H), 3.87 (s, 3H). FT-IR(ATR): 900 cm^{-1} (νR–O═U═O), 2900 cm^{-1} (νR–CH), 3300 cm^{-1} (νR–NH), 3500 cm^{-1} (νR–OH_2). ESI + MS *m*/*z* (M + H): calc: 842.557 found: 845.3752. Elemental analysis: calc: C (41.82), H (4.09), N (9.75); found C (42.12), H (3.91), N (9.43). Formula: $C_{22}H_{17}N_4O_7U\cdot2(C_4H_9NO)$.

Synthesis of CN salimidizine (L4)-Cu complex. (**L4**) (0.049 mmol; 16.4 mg) was dissolved in a mixture of 12 mL DMF/8 mL of H_2O and was allowed to stir for 20 min at 50 °C to help dissolve the ligand. Next copper(II) acetate (0.049 mmol; 9.0 mg) was added to the reaction, followed by triethylamine (0.098 mmol; 20 μL) to assist in deprotonation of the ligand. The reaction was heated to 100 °C and allowed to react for 48 hours. The reaction was followed by TLC by 3 : 1 EtOAc : Hex mixture. The reaction was then taken to dryness under high vac at 70 °C to yield a black solid the solid was scraped from the round bottomed flask and washed with EtOH and filtered (21.0 mg). Yield: 93%. FT-IR (ATR): 2200 cm^{-1} (νC≡N), 2900 cm^{-1} (νR–CH), 3100 cm^{-1} (νR–OH_2), 3300 cm^{-1} (νR–NH). ESI + MS *m*/*z*(M + H): calc: 457.024, found: 458.100; elemental analysis: calc: C (52.03), H (3.64), N (12.65); found C (51.74), H (3.35), N (12.97). Formula: $C_{22}H_{14}N_5O_4Cu\cdot(C_2H_6OS)$.

Synthesis of CN salimidizine (L4)-UO_2 complex. (**L4**) (0.050 mmol; 16.4 mg) was dissolved in a mixture of 12 mL DMF/8 mL of H_2O and was allowed to stir for 20 min at 50 °C to help dissolve the ligand. Next, uranyl acetate dihydrate (0.050 mmol; 21.0 mg) was added to the reaction, followed by triethylamine (0.000098 mol; 20 μL) to assist in deprotonation of the ligand. The reaction was heated to 100 °C and allowed to react for 48 hours. The reaction was then taken to dryness under high vac at 70 °C to yield a brown solid, the solid was scraped from the round bottom and washed with EtOH and filtered (28.3 mg). Yield: 83%, NMR (500 MHz, DMF-d7, ppm): δ10.23 (s, 3H), 8.86 (s, 1H), 8.54–8.25 (m, 3H), 7.88 (s, 4H), 3.51(bs, 3H), 1.28 (s, (3H)). FT-IR (ATR): 850 cm^{-1} (νR–O═U═O), 2200 cm^{-1} (νC≡N), 2900 cm^{-1} (νR–CH), 3100 cm^{-1} (νR–OH_2), 3300 cm^{-1} (νR–NH). ESI + MS *m*/*z*(M + Na): calc: 819.214, found: 819.1835; elemental analysis: calc: C (40.34), H (3.51), N (8.40); found C (40.40), H (3.62), N (8.34). Formula: $C_{24}H_{20}N_4O_9U\cdot2(C_4H_9NO)$.

Conclusions

In conclusion, four derivatives of 2-(1*H*-imidazo[4,5-*b*]phenazin-2-yl)phenol, (salimidizine) **L1** and (di *t*-butylsalimidizine) **L2**, (cyanosalimidizine) **L3**, and (methoxysalimidizine) **L4** have been synthesized. Metal complex UO_2[**L1**](OAc)·DMSO complex was characterized in the solid state as well as free base of **L1** and **L2**. Ligands **L1**, **L2**, **L3**, and **L4** were characterized using Ultraviolet–Visible absorbance and emission spectroscopies with uranyl and copper. An increase in absorption, in the case of UO_2^{2+} and two new modes of absorbance were observed in the case of Cu. In the presence of greater than a 1 to 1 ratio of UO_2 : ligand, the emission more than doubled; in contrast, in the presence of any ratio of Cu : ligand emission was quenched by at least half. Based on the calculated potential energy profiles, we were able to explain these observations. The minimum of the pertinent excited electronic state for copper is shallow, and decays readily to a different minimum with zero oscillator strength, and thus, the decay to the ground state follows a non-radiative path is indicates a degree of promise in the foundation of a selective fluorescent indicator for uranyl, as most other examples of these systems selectively quench in the presence of transition metals.

Conflicts of interest

There are no conflicts of interest or competing interests to declare.

Acknowledgements

We would like to thank Patrick Donnan and Prof. Steve Mansoorabadi for their invaluable assistance in running and deconvoluting of the calculations for this manuscript. This work was completed with resources provided by the Auburn University Hopper Cluster and the National Energy Research Scientific Computing Center (NERSC), a U.S. Department of Energy Office of Science User Facility operated under Contract DE-AC02-05CH11231. The authors would like to acknowledge that this work was funded by the United States Department of Energy – Basic Energy Sciences through the Chemical Sciences, Geosciences, and Biosciences (CSGB) subdivision for Heavy Elements Chemistry with Award DE-SC0019177 to Auburn University.

Notes and references

1 G. Yadav and S. Ganguly, Structure Activity Relationship (SAR) Study of Benzimidazole Scaffold for Different Biological Activities: A Mini-Review, *Eur. J. Med. Chem.*, 2015, **97**, 419–443, DOI: 10.1016/j.ejmech.2014.11.053.

2 S. M. Sondhi, J. Singh, P. Roy, S. K. Agrawal and A. K. Saxena, Conventional and Microwave-Assisted Synthesis of Imidazole and Guanidine Derivatives and

Their Biological Evaluation, *Med. Chem. Res.*, 2011, **20**(7), 887–897, DOI: 10.1007/s00044-010-9410-6.

3 A. K. Boudalis, J. M. Clemente-Juan, F. Dahan, V. Psycharis, C. P. Raptopoulou, B. Donnadieu, Y. Sanakis and J.-P. Tuchagues, Reversible Core-Interconversion of an Iron (III) Dihydroxo Bridged Complex, *Inorg. Chem.*, 2008, **47**(23), 11314–11323, DOI: 10.1021/ic800716r.

4 Y.-P. Tong, S.-L. Zheng and X.-M. Chen, Structures, Photoluminescence and Theoretical Studies of Two ZnII Complexes with Substituted 2-(2-Hydroxyphenyl) Benzimidazoles, *Eur. J. Inorg. Chem.*, 2005, **2005**(18), 3734–3741, DOI: 10.1002/ejic.200500174.

5 M. R. Maurya, M. Kumar and U. Kumar, Polymer-Anchored Vanadium(IV), Molybdenum(VI) and Copper(II) Complexes of Bidentate Ligand as Catalyst for the Liquid Phase Oxidation of Organic Substrates, *J. Mol. Catal. A: Chem.*, 2007, **273**(1), 133–143, DOI: 10.1016/j.molcata.2007.03.074.

6 J. Ouyang, H. Hong, C. Shen, Y. Zhao, C. Ouyang, L. Dong, J. Zhu, Z. Guo, K. Zeng, J. Chen, C. Zhang and J. Zhang, A Novel Fluorescent Probe for the Detection of Nitric Oxide in Vitro and in Vivo, *Free Radicals Biol. Med.*, 2008, **45**(10), 1426–1436, DOI: 10.1016/j.freeradbiomed.2008.08.016.

7 G. Gao, W. Qu, B. Shi, P. Zhang, Q. Lin, H. Yao, W. Yang, Y. Zhang and T. Wei, A Highly Selective Fluorescent Chemosensor for Iron Ion Based on 1H-Imidazo [4,5-b] Phenazine Derivative, *Spectrochim. Acta, Part A*, 2014, **121**, 514–519, DOI: 10.1016/j.saa.2013.11.004.

8 M. A. Katkova, T. V. Balashova, V. A. Ilichev, A. N. Konev, N. A. Isachenkov, G. K. Fukin, S. Yu. Ketkov and M. N. Bochkarev, Synthesis, Structures, and Electroluminescent Properties of Scandium N,O-Chelated Complexes toward Near-White Organic Light-Emitting Diodes, *Inorg. Chem.*, 2010, **49**(11), 5094–5100, DOI: 10.1021/ic1002429.

9 M. A. Katkova, A. P. Pushkarev, T. V. Balashova, A. N. Konev, G. K. Fukin, S. Yu. Ketkov and M. N. Bochkarev, Near-Infrared Electroluminescent Lanthanide [Pr(Iii), Nd(Iii), Ho(Iii), Er(Iii), Tm(Iii), and Yb (Iii)] N,O-Chelated Complexes for Organic Light-Emitting Devices, *J. Mater. Chem.*, 2011, **21**(41), 16611–16620, DOI: 10.1039/C1JM13023D.

10 M. Massacesi and G. Ponticelli, Spectroscopic Studies of Cobalt(II), Nickel(II) and Copper(II) Complexes with N-Ethyl- and N-Propylimidazole, *J. Inorg. Nucl. Chem.*, 1974, **36**(10), 2209–2217, DOI: 10.1016/0022-1902(74)80257-5.

11 S. M. Prakash, K. Jayamoorthy, N. Srinivasan and K. I. Dhanalekshmi, Fluorescence Tuning of 2-(1H-Benzimidazol-2-Yl)Phenol-ESIPT Process, *J. Lumin.*, 2016, **172**, 304–308, DOI: 10.1016/j.jlumin.2015.12.009.

12 A. E. V. Gorden, M. A. DeVore and B. A. Maynard, Coordination Chemistry with F-Element Complexes for an Improved Understanding of Factors That Contribute to Extraction Selectivity, *Inorg. Chem.*, 2013, **52**(7), 3445–3458, DOI: 10.1021/ic300887p.

13 M. A. DeVore II, S. A. Kerns and A. E. V. Gorden, Characterization of Quinoxolinol Salen Ligands as Selective Ligands for Chemosensors for Uranium, *Eur. J. Inorg. Chem.*, 2015, **2015**(34), 5708–5714, DOI: 10.1002/ejic.201501033.

14 M. Azam, S. I. Al-Resayes, G. Velmurugan, P. Venuvanalingam, J. Wagler and E. Kroke, Novel Uranyl (vi) Complexes Incorporating Propylene-Bridged Salen-Type N2O2-Ligands: A Structural and Computational Approach, *Dalton Trans.*, 2015, **44**(2), 568–577, DOI: 10.1039/C4DT02112F.

15 M. Azam, S. I. Al-Resayes, A. Trzesowska-Kruszynska, R. Kruszynski, S. Mohammad Wabaidur, S. M. Soliman, R. K. Mohapatra and M. Rizwan Khan, Dinuclear Uranyl Coordination Compound: Structural Investigations and Selective Fluorescence Sensing Properties, *Polyhedron*, 2020, **189**, 114745, DOI: 10.1016/j.poly.2020.114745.

16 L. Mello, S. dos, J. W. da Cruz Jr., D. H. Bucalon, S. Romera, M. P. dos Santos, L. M. Lião, L. Vizotto, F. T. Martins and E. R. Dockal, Synthesis, Characterization and Crystal Structure of Racemic Vanadyl and Uranyl Salen-Type Complexes, *J. Mol. Struct.*, 2021, **1228**, 129656, DOI: 10.1016/j.molstruc.2020.129656.

17 A. M. Amer, A. A. El-Bahnasawi, M. R. H. Mahran and M. Lapib, On the Synthesis of Pyrazino[2,3-b]phenazine and 1H-Imidazo[4,5b] phenazine Derivatives, *Monatsh. Chem.*, 1999, **130**, 1217–1225.

18 Y. J. Lei, D. Q. Li, J. Ouyang and J. X. Shi, Synthesis and Optical Properties of 2-(1H-Imidazo [4,5-] Phenazin-2-Yl) Phenol Derivatives, *Adv. Mater. Res.*, 2011, **311–313**, 1286–1289, DOI: 10.4028/www.scientific.net/AMR.311-313.1286.

19 P.-Y. Gu, C. Wang, L. Nie, G. Long and Q. Zhang, A Novel Heteroacene 2-(Perfluorophenyl)-1H-Imidazo[4,5-b] Phenazine for Selective Sensing of Picric Acid, *RSC Adv.*, 2016, **6**(44), 37929–37932, DOI: 10.1039/C6RA08547D.

20 B. Shi, P. Zhang, T. Wei, H. Yao, Q. Lin, J. Liu and Y. Zhang, A Reversible Fluorescent Chemosensor for Mercury Ions Based on 1H-Imidazo[4,5-b]Phenazine Derivatives, *Tetrahedron*, 2013, **69**(37), 7981–7987, DOI: 10.1016/j.tet.2013.07.007.

21 J. L. Sessler, P. J. Melfi, D. Seidel, A. E. V. Gorden, D. K. Ford, P. D. Palmer and C. D. Tait, Hexaphyrin (1.0.1.0.0.0). A New Colorimetric Actinide Sensor, *Tetrahedron*, 2004, **60**(49), 11089–11097, DOI: 10.1016/j.tet.2004.08.055.

22 M. S. Kim and T. Tsukahara, Studies on Coordination and Fluorescence Behaviors of a Novel Uranyl Ion-Selective Chemosensor Bearing Diaza 18-Crown-6 Ether and Naphthalimide Moieties, *ACS Earth Space Chem.*, 2020, **4**(12), 2270–2280, DOI: 10.1021/acsearthspacechem.0c00184.

23 V. V. Halali and R. G. Balakrishna, An Expeditious Method for the Ultra-Level Chemosensing of Uranyl Ions, *Anal. Methods*, 2020, **12**(8), 1070–1076, DOI: 10.1039/C9AY02715G.

24 Q. Hu, W. Zhang, Q. Yin, Y. Wang and H. Wang, A Conjugated Fluorescent Polymer Sensor with Amidoxime and Polyfluorene Entities for Effective Detection of Uranyl

Ion in Real Samples, *Spectrochim. Acta, Part A*, 2021, **244**, 118864, DOI: 10.1016/j.saa.2020.118864.

25 K. Takao, M. Kato, S. Takao, A. Nagasawa, G. Bernhard, C. Hennig and Y. Ikeda, Molecular Structure and Electrochemical Behavior of Uranyl(VI) Complex with Pentadentate Schiff Base Ligand: Prevention of Uranyl(V) Cation−Cation Interaction by Fully Chelating Equatorial Coordination Sites, *Inorg. Chem.*, 2010, **49**(5), 2349–2359, DOI: 10.1021/ic902225f.

26 Z. Asadi, M. Asadi, A. Zeinalli, M. Ranjkeshshorkaei, K. Fejfavova, V. Eigner, M. Dusek and A. Dehnokhalaji, Synthesis Structural Investigation and Kinetic Studies of Uranyl(VI) Unsymmetrical Schiff Base Complexes, *J. Chem. Sci.*, 2014, **126**(6), 1673–1683, DOI: 10.1007/s12039-014-0720-y.

27 Y. Suzuki and H. Takahashi, Formyaltion of Phenols with Electron-Withdrawing Groups in Strong Acids. Synthesis of Substituted Salicylaldehydes, *Chem. Pharm. Bull.*, 1983, **31**(5), 1751–1753.

28 G. M. Sheldrick, A Short History of It SHELX, *Acta Crystallogr., Sect. A: Found. Crystallogr.*, 2008, **64**(1), 112–122, DOI: 10.1107/S0108767307043930.

29 O. V. Dolomanov, L. J. Bourhis, R. J. Gildea, J. A. K. Howard and H. Puschmann, It OLEX2: A Complete Structure Solution, Refinement and Analysis Program, *J. Appl. Crystallogr.*, 2009, **42**(2), 339–341, DOI: 10.1107/S0021889808042726.

30 A. D. Becke, Density-Functional Exchange-Energy Approximation with Correct Asymptotic Behavior, *Phys. Rev. A*, 1988, **38**(6), 3098–3100, DOI: 10.1103/PhysRevA.38.3098.

31 C. Lee, W. Yang and R. G. Parr, Development of the Colle-Salvetti Correlation-Energy Formula into a Functional of the Electron Density, *Phys. Rev. B: Condens. Matter Mater. Phys.*, 1988, **37**(2), 785–789, DOI: 10.1103/PhysRevB.37.785.

32 T. H. Dunning, Gaussian Basis Sets for Use in Correlated Molecular Calculations. I. The Atoms Boron through Neon and Hydrogen, *J. Chem. Phys.*, 1989, **90**(2), 1007–1023, DOI: 10.1063/1.456153.

33 N. B. Balabanov and K. A. Peterson, Systematically Convergent Basis Sets for Transition Metals. I. All-Electron Correlation Consistent Basis Sets for the 3d Elements Sc–Zn, *J. Chem. Phys.*, 2005, **123**(6), 064107, DOI: 10.1063/1.1998907.

34 K. A. Peterson, Correlation Consistent Basis Sets for Actinides. I. The Th and U Atoms, *J. Chem. Phys.*, 2015, **142**(7), 074105, DOI: 10.1063/1.4907596.

35 M. J. Frisch, G. W. Trucks, H. B. Schlegel, G. E. Scuseria, M. A. Robb, J. R. Cheeseman, G. Scalmani, V. Barone, G. A. Petersson, H. Nakatsuji, X. Li, M. Caricato, A. V. Marenich, J. Bloino, B. G. Janesko, R. Gomperts, B. Mennucci, H. P. Hratchian, J. V. Ortiz, A. F. Izmaylov, J. L. Sonnenberg, D. Williams-Young, F. Ding, F. Lipparini, F. Egidi, J. Goings, B. Peng, A. Petrone, T. Henderson, D. Ranasinghe, V. G. Zakrzewski, J. Gao, N. Rega, G. Zheng, W. Liang, M. Hada, M. Ehara, K. Toyota, R. Fukuda, J. Hasegawa, M. Ishida, T. Nakajima, Y. Honda, O. Kitao, H. Nakai, T. Vreven, K. Throssell, J. A. Montgomery Jr., J. E. Peralta, F. Ogliaro, M. J. Bearpark, J. J. Heyd, E. N. Brothers, K. N. Kudin, V. N. Staroverov, T. A. Keith, R. Kobayashi, J. Normand, K. Raghavachari, A. P. Rendell, J. C. Burant, S. S. Iyengar, J. Tomasi, M. Cossi, J. M. Millam, M. Klene, C. Adamo, R. Cammi, J. W. Ochterski, R. L. Martin, K. Morokuma, O. Farkas, J. B. Foresman and D. J. Fox, *Gaussiañ16 Revision C.01*, 2016.